

Supporting information

Cofactor specificity engineering of a long chain secondary alcohol dehydrogenase from *Micrococcus luteus* for redox-neutral biotransformation of fatty acids

Eun-Ji Seo,^a Hye-Ji Kim,^b Myeong-Ju Kim,^a Jeong-Sun Kim,^{b,*} and Jin-Byung Park,^{a,*}

^a.Department of Food Science & Engineering, Ewha Womans University, Seoul 03760, Republic of Korea. E-mail: jbpark06@ewha.ac.kr

^b.Department of Chemistry, Chonnam National University, Gwangju 61186, Republic of Korea. E-mail: jsunkim@chonnam.ac.kr

Table of Contents

Experimental procedures

Microbial strains, culture conditions and protein expression

Reagents

Activity assay of alcohol dehydrogenase

Structure determination of alcohol dehydrogenase

Characterization of the extreme C-terminal region (Gly288-Gly310)

Sequence alignments

Modeling of the alcohol dehydrogenase-NAD⁺ complex

Reconstruction of NAD⁺-binding region of alcohol dehydrogenase

Site-directed mutagenesis

Purification of engineered enzymes

Cofactor specificity and substrate specificity of the engineered alcohol dehydrogenases

Two-step biotransformations

Product analysis by gas chromatography/mass spectrometry

Supplementary Tables

Table S1. Plasmid and strains used in this study

Table S2. Primers used in this study

Table S3. Data collection and structure refinement statistics

Table S4. Kinetic constants of alcohol dehydrogenase and its variants

Table S5. The engineering targets, which have been suggested by the CSR-SALAD analysis

Table S6. Substrate Specificity for alcohol dehydrogenase and its variants

Supplementary Schemes

Scheme S1. Redox self-sustaining biotransformation of cyclohexanol into ϵ -caprolactone

Scheme S2. Designed biotransformation pathway of oleic acid

Scheme S3. The two-step biotransformation of 10,12-dihydroxyoctadecanoic acid

Supplementary Figures

Figure S1. A cartoon representation of the alcohol dehydrogenase dimer in the X-ray crystal structure

Figure S2. Active site of alcohol dehydrogenase

Figure S3. Active site of alcohol dehydrogenase with non-protein molecules

Figure S4. The extreme C-terminal region of mLSADH (Gly288-Gly310)

Figure S5. The superposed crystal structures of alcohol dehydrogenase and Cyclohexadienyl dehydrogenase

Figure S6. The k_{cat}/K_M and K_M values for NAD(P)⁺ of the purified enzymes

Experimental procedures

Microbial strains, culture conditions and protein expression

The recombinant *Escherichia coli* BL21(DE3), expressing the recombinant enzymes including the secondary alcohol dehydrogenase of *M. luteus* (mLSADH) and the engineered Baeyer-Villiger monooxygenase (i.e., E6BVMO_C302I) of *P. putida* KT2440¹⁻⁵ were cultivated overnight in the lysogeny broth (LB) medium supplemented with appropriate antibiotics for seed cultivation (Table S1). The Riesenberg medium supplemented with 10 g/L glucose and the appropriate antibiotics was used for the main cultivation. The recombinant genes in the pACYC- and the pETDuet-vectors were expressed by adding 0.1 mM isopropyl β -D-1-thiogalactopyranoside (IPTG) into the cultivation medium.

Reagents

Ricinoleic acid, 12-hydroxyoctadecanoic acid, and palmitic acid were purchased from Tokyo Chemical Industry Co. (Tokyo, Japan). 10-Hydroxyoctadecanoic acid, 10,12-dihydroxyoctadecanoic acid, 10-ketooctadecanoic acid, and 10-keto-12-hydroxyoctadecanoic acid were prepared in our lab according to the previous studies.^{1,3} 4-Decanone, 4-decanol, 2-decanol, 1-decanol, 3-nonanol, 2-nonanol, and 1-nonanol were obtained from Tokyo Chemical Industry Co. (Tokyo, Japan). *N*-Methyl-*N*-(trimethylsilyl)trifluoroacetamide (TMS) and NAD(P)⁺ were purchased from Tokyo Chemical Industry Co. (Tokyo, Japan). Ethyl acetate was purchased from Duksan Pure Chemical Co. (Ansan, Republic of Korea). Glucose was obtained from Junsei Chemical Co (Tokyo, Japan). Antibiotics, trace elements for culture medium, FAD, and Tween80 were purchased from Sigma (St. Louis, MO, USA).

mLSADH activity assay

The mLSADH activity was measured based on a previous study.³ In brief, the activity was determined by monitoring NAD⁺ consumption at 340 nm for 180 s in 1 mL cuvettes using a spectrophotometer (Thermo Fisher Scientific, MA, USA). Assays were performed in 50 mM sodium pyrophosphate buffer (pH 9.0), containing 0.5 mM NADPH, 5 mM 4-decanol, and an appropriate amount of crude enzyme extract. One unit (U) of enzyme activity was defined as the amount of enzyme required to reduce 1 μ mol of NAD⁺ for 1 min under the assay reaction conditions.

Structure determination of mLSADH

The purified mLSADH was concentrated up to 24.4 mg·mL⁻¹ for crystallization in the buffer consisting of 20 mM Tris-HCl at pH 7.5 and 200 mM NaCl. Protein concentration was determined by measuring the UV absorbance and considering the extinction coefficient of 1.748 mg·mL⁻¹·cm⁻¹ at 280 nm, which was calculated from its amino acid sequence. Crystallization attempts that were performed at 22 °C by the sitting-drop vapor-diffusion method. Initial crystallization hits found using the Hampton crystal screen was optimized by a grid search using 24-well Linbro plates and the hanging-drop vapor-diffusion method at 22 °C, where 1 μ l protein and 1 μ l reservoir solution were mixed together and equilibrated with 0.2 ml precipitant containing 1.0 M tri-sodium citrate dihydrate at pH 6.5. For diffraction experiments, crystals were briefly immersed into the precipitant solution containing additional 15 % (v/v) glycerol as the cryo-protectant and immediately placed in the 100 K liquid nitrogen-gas stream. The

diffraction data were collected at the 11C beam line of the Pohang Accelerator Laboratory (PAL, Korea) with the per-frame oscillation of 1° and per-frame exposure of 1 s. A total of 360 images of each complexed crystal were collected on the Pilatus 6M detector. The indexing, integration, and scaling of the reflections were conducted using HKL2000 suite.⁶ The crystal structure was solved by a molecular replacement program PHENIX⁷ using the diketoreductase from *Homo sapiens* (PDB ID 4e13) as an initial search model. Further model building was performed manually using WinCoot⁸, and subsequent refinement was performed with PHENIX.⁷ The data and refinement statistics are summarized in Table S3. The quality of the model was analyzed by using WinCoot⁸ and MolProbity⁹. Coordinates and structure factors have been deposited in the PDB with the accession numbers 6KQ9 and 6KQB.

Characterization of the extreme C-terminal region (Gly288-Gly310)

Sequence comparison of mLSADH with the functionally related proteins reveals a remarkable difference at the extreme C-terminal region (eC-term) of mLSADH (Fig. S4). Characteristically, this region of ~20 residues in mLSADH includes a number of acidic residues of Asp290, Glu292, Glu298, Asp299, Asp304, and Asp306. Deletion of this region invoked aggregation of the expressed recombinant protein (Fig. S4). These 20 residues form a pair of short β -strands (Tyr285-Pro296; β 9 and β 10) and an extended structure (Val297-Gly310) in the revealed mLSADH structure (Fig. S4) and interact with the remaining part of the protein. The β -sheet forms the substrate-binding cleft, together with the α 2-helix, whereas the extended region of the eC-term (Val297-Gly310) interact with the outer hydrophobic pocket within the C-terminal domain.

However, the characteristic acidic residues within this eC-term are exposed to solvent without formation of any interaction with the other part of the protein.

Sequence alignments

Sequence alignment was performed in the NCBI blastp using the Protein Data Bank database. Program algorithms including Position-Specific Iterated BLAST (PSI-BLAST) and Domain Enhanced Lookup Time Accelerated BLAST (DELTA-BLAST) were used.

Modeling of the mLSADH-NAD⁺ complex

The NAD⁺ binding model of mLSADH was created using the Maestro visualization tool. The revealed mLSADH structure was superposed on the AbDKR structure with the bound NAD⁺ cofactor, and then the NAD⁺ cofactor was transferred on the mLSADH surface. The mLSADH and NAD⁺ complex model was further energy-minimized to get the final NAD⁺-bound model of mLSADH.

Reconstruction of the NAD⁺-binding pocket of mLSADH

All mutant structures were prepared by *in silico* mutations based on the homology modeled mLSADH structure, with structure refinement using Protein Preparation Wizard, Epik, and Prime modules in the Schrödinger software package, based on the OPLS3 forcefield.¹⁰⁻¹² The resulting structures of mutants were analyzed for intramolecular interactions including hydrogen bonds, aromatic hydrogen bonds, salt bridges, pi-pi stacking and pi-cation interactions by Maestro program. To alter the cofactor specificity from NAD⁺ to NADP⁺, structural analysis strategy has been applied.

According to cofactor binding site of the modeled structure of mLSADH, two residues (D37, V39) were selected to engineering target for decreasing the charge repulsion and structural hindrance (Fig S5), which were replaced with the hydrophilic serine residues (Table S2).

To further increase the enzyme affinity for NADP⁺, the “Cofactor Specificity Reversal-Structural Analysis and Library Design” (CSR-SALAD), a web tool intended to design the enzymes with reversed NAD(P)⁺ specificity¹³, has been used. Homology model of mLSADH with bound NAD⁺ in the PDB format and the PDB file of homologous protein, diketoreductase from *A. baylyi* (PDB code 4dyd), were submitted into the CSR-SALAD web site. The total 5 positions including A38 as a common target residue were recommended as the engineering targets (Table S5). Based on the CSR-SALAD analysis, triple and quadruple mutants were constructed and examined.

Site-directed mutagenesis

The site-directed mutagenesis of mLSADH was performed by PCR using KOD Xtreme™ Hot Start DNA Polymerase (Novagen), according to manufacturer's instructions. Briefly, the PCR reaction mixtures (50 μL) consisted of 2X Xtreme Buffer (25 μL), deoxynucleoside triphosphates (0.4 mM each), KOD Xtreme™ Hot Start DNA Polymerase (1 U), plasmid DNA (10 ng), and both sense and anti-sense primers (10 μM) (Table S2). The PCR was started with an initial denaturation step at 94 °C for 2 min, followed by 25 cycles of denaturing at 98 °C for 10 s, annealing at 60 °C for 30 s, and extension at 68 °C for 6.5 min, with a final extension at 68 °C for 10 min. After gel purification (Elpis Biotech, Daejeon, Korea), PCR products were digested with 0.4 U of DpnI (New England Biolabs, Ipswich, MA, USA) at 37 °C for 1 h, to ensure removal

of the plasmid DNA template. DNA fragments were then purified by gel purification, followed by transformation into *E. coli* DH5 α cells. After overnight cultivation on agar medium, random colonies were selected and mutagenesis was confirmed through sequencing.

Purification of the engineered mLSADHs and BVMO

The recombinant *E. coli* BL21(DE3) expressing the engineered mLSADHs (i.e., mLSADH-D37S/V39S and mLSADH-T15I/D37S/A38R/V39S) or BVMO (i.e., E6BVMO_C302I) were cultivated in the Riesenberg medium, after which they were harvested through centrifugation at 5,000 g for 15 min and washed with Tris-HCl (pH 8, 50 mM). The washed cells were resuspended into the Tris-HCl buffer and subjected to the cell lysis by sonication. Afterwards, the resulting enzymes were purified via affinity chromatography on a Ni-NTA gel matrix (Qiagen, Crawley, United Kingdom). 1 mL of Ni-NTA slurry (0.5 mL bed volume) was equilibrated with 2 mL of lysis buffer (50 mM NaH₂PO₄, 300 mM NaCl, 10 mM imidazole, pH 8.0), and the cleared lysate was added to this equilibrated matrix, and this mixture was mixed gently at 4 °C for 60 min. The lysate-Ni-NTA mixture was loaded into a column. The column was washed with 10 bed volume of wash buffer (50 mM NaH₂PO₄, 300 mM NaCl, 20 mM imidazole, pH 8.0). The target proteins were then eluted by increasing the imidazole concentration to 0.25 M. Fractions containing the recombinant proteins were pooled and dialyzed to remove imidazole.

Cofactor specificity and affinity of the engineered mLSADH

Cofactor specificity of the engineered mLSADH enzymes was evaluated by NADPH assay in the presence of 0.3 mM 10-hydroxyoctadecanoic acid as the substrate and various concentrations of NAD(P)⁺ in 50 mM Sodium pyrophosphate buffer (pH 9.0). Substrate specificity of the engineered mLSADH enzymes was also evaluated by NADPH assay in the presence of 0.5 mM NAD(P)⁺ and various concentrations of reaction substrates in 50 mM Sodium pyrophosphate buffer (pH 9.0). The cofactor consumption was measured for 3 min at 340 nm. One unit (U) of the enzyme activity was defined as the amount of enzyme to reduce 1 μmol of NAD(P)⁺ for 1 min under the reaction condition.

Two-step biotransformations

The biotransformation was carried out in a 15mL conical tube containing the reaction buffer (50 mM Tris-HCl, pH 8.0), NADP⁺ (0.2-1.0 mM), 0.2 mM FAD, 0.5 g/L Tween 80, 5 mM reaction substrate (i.e., 10,12-dihydroxyoctadecanoic acid and 10-hydroxyoctadecanoic acid), 0.25 μM mLSADH mutants and 200 μM BVMO variant for 1 hour at 30 °C.

Product analysis by gas chromatography/mass spectrometry (GC/MS)

Concentrations of the fatty acids, fatty alcohols and their derivatives were measured as described previously.³ The reaction medium was mixed with a twice volume of ethyl acetate containing palmitic acid as an internal standard. The organic phase was harvested after vigorous vortexing and was then subjected to derivatization with N-methyl-N-(trimethylsilyl) trifluoroacetamide (TMS). The TMS derivatives were analyzed by GC/MS (Agilent, Santa Clara, CA, USA) equipped with a flame ionization

detector and a split injection system (split ratio set at 1:10) and fitted with a nonpolar capillary column (30 m length, 0.25- μ m thickness, HP-5MS, Agilent Technologies, Palo Alto, CA, USA). Column temperature was increased from 90 to 255°C at a rate of 5 °C/min, and then maintained at 255 °C. The injector and detector temperatures were 260 and 250 °C, respectively. Mass spectra were obtained by electron impact ionization at 70 eV. Scan spectra were obtained within the range of 100–600 m/z. Selected ion monitoring (SIM) was used for the detection and fragmentation analysis of the reaction products.

Supplementary Tables

Table S1. Plasmid and strains used in this study.

Name	Relevant characteristics	Source
Strains		
BL21(DE3)	<i>E. coli</i> F ⁻ <i>ompT gal dcm lon hsdSB</i> (rB ⁻ mB ⁻) λ(DE3)	Invitrogen
BL21(DE3)	BL21(DE3) /pACYC-ADH-FadL	14
BL21(DE3)	BL21(DE3) /pACYC- ADH_D37S/V39S-FadL	This study
BL21(DE3)	BL21(DE3) /pACYC- ADH_D37S/A38R/V39S- FadL	This study
BL21(DE3)	BL21(DE3) /pACYC- ADH_D37S/A38R/V39S/T15I- FadL	This study
BL21(DE3)	BL21(DE3) /pET-E6BVMO_C302I	3

Plasmids		
pETDuet	Expression vector, Amp ^R , pMB1 ori	Novagen
pACYCDuet	Expression vector, Cm ^R , p15A ori	Novagen
pACYC-ADH-FadL	pACYC-P _{T7} -ADH-P _{T7} -FadL-T _{T7}	14
pACYC- ADH_D37S/V39S- FadL	pACYC-P _{T7} -ADH-P _{T7} -FadL-T _{T7}	This study
pACYC- ADH_D37S/A38R/V 39S-FadL	pACYC-P _{T7} -ADH-P _{T7} -FadL-T _{T7}	This study
pACYC- ADH_D37S/A38R/V 39S/T15I-FadL	pACYC-P _{T7} -ADH-P _{T7} -FadL-T _{T7}	This study
pET-E6BVMO_ C302I	pET-P _{T7} -E6BVMO_C302I-T _{T7}	3

Table S2. Primers used in this study.

Name	Sequence (5'-3')
D37S/V39S	GGTGATGGCCTACAGCGCCAGCCCCGCCGCCCTCG
D37S/A38R /V39S	GATGGCCTACAGCCGTAGCCCCGCCGCC
D37S/A38R /V39S/T15I	GTCGCCGTGCTGGGCATTGGCGTGCTGG
N198A	GATCCCGGGCTACTTCCTCGCCTCCCTGCTCATCCCG
R151E	GCCCTGCACTACGCCAACGAGATCTGGGCGCAGAACACC
R234E	GTGGCCACCGGCAACGAGGAGGGCCCGTTCCAGACCTAC
N150A	CTGGCCCTGCACTACGCCGCCCGCATCTGGGCGCAGAAC
T239M	GAGCGCGGCCCGTTCCAGATGTACGACATCGTGGGCTTC
Q155E	GCCAACCGCATCTGGGCGGAGAACACCGCCGAGGTCA
V251W	TTCCACGTGGCCGCCAACTGGTCCCGCAACACGGGCGTC
H147A	GAGCGCTTCCTGGCCCTGGCCTACGCCAACCGCATCTGG
E159A	GGGCGCAGAACACCGCCGCGGTCATGGGCACCGCCGC

Table S3. Data collection and structure refinement statistics.

Data Collection	mLSADH	Dimeric mLSADH
Space group	P3 ₁ 21	P3 ₂ 21
Unit cell dimensions		
a, b, c (Å),	65.13, 65.13, 165.21,	64.49, 64.49, 321.54,
α , β , γ (°)	90, 90, 120	90, 90, 120
Wavelength (Å)	0.9793	1.0000
Resolution (Å)	50-2.27 (2.31-2.27) ^a	50-2.26 (2.30-2.26) ^a
$R_{p.i.m.}$	4.8 (47.8)	4.5 (25.0)
$I/\sigma(I)$	29 (2.3)	11.4 (2.0)
Completeness (%)	99.9 (99.3)	100 (99.9)
Redundancy	8.3 (6.7)	17.3 (14.9)
Refinement		
No. of reflections	19445	37668
R_{work} / R_{free}	20.0 (27.7) / 21.7 (30.3)	21.6 (28.6) / 23.7 (35.6)
No. protein molecules	1	2
No. atoms		
protein / water	2381 / 143	4774 / 142
R.m.s. deviations		
bond lengths (Å) / angles (°)	0.002 / 0.49	0.003 / 0.60
Average B-values (Å ²)		
protein / water	23.5 / 29.2	25.5 / 26.3
Ramachandran plot (%)		
favoured / allowed / outliers	96.5 / 3.2 / 0.3	97.6 / 2.2 / 0.2

^a The numbers in parentheses are the statistics from the highest resolution shell.

Table S4. Kinetic constants of mLSADH and its variants.

	V_{\max} (mM s ⁻¹)	K_M (mM)	k_{cat} (s ⁻¹)	k_{cat}/K_M (μM^{-1} s ⁻¹)
Wild-type	0.00223	39.27992	150.6757	3.835947
N198A	5.43E-04	199.5859	1.83E+00	0.009162
R151E	2.79E-03	92.41083	9.39E+01	1.016541
R234E	6.85E-03	92.16409	2.31E+02	2.50249
R151E/R234E	1.11E-03	129.8883	3.74E+01	0.287737
N150A	1.44E-03	154.113	4.85E+01	0.314606
T239M	1.77E-03	467.8254	5.96E+01	0.127389
Q155E	2.31E-03	186.2234	7.78E+01	0.417658
V251W	1.66E-03	291.3378	2.81E-01	0.000966
H147A	2.89E-05	200.9024	1.95E-02	9.71E-05
E159A	1.17E-04	270.6407	7.89E-02	0.000291

Table S5. The engineering targets, which have been suggested by the CSR-SALAD analysis.

(A) The structural model of mLSADH in complex with NAD⁺ was used as the template.

Residue	Codon	Possible amino acids
ASP 37	VMC	ADHNPT
ALA 42	RSA	AGRT
ARG 49	MRK	HKNQRS

(B) The diketoreductase from *A. baylyi* (PDB code 4dyd) with 47.5 % sequence identity with mLSADH was used as the template.

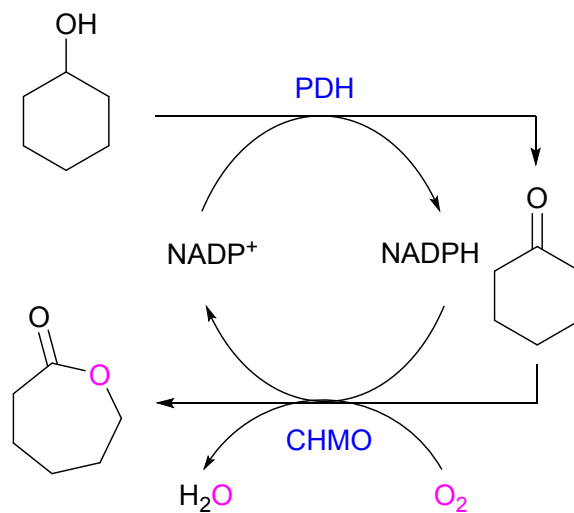
Residue	Codon	Possible amino acids
THR 15	DCA	AST
ASP 37	RNC	ADGINSTV
ALA 38	ANA	IKRT

Table S6. Substrate Specificity for wild-type mLSADH and its variants.

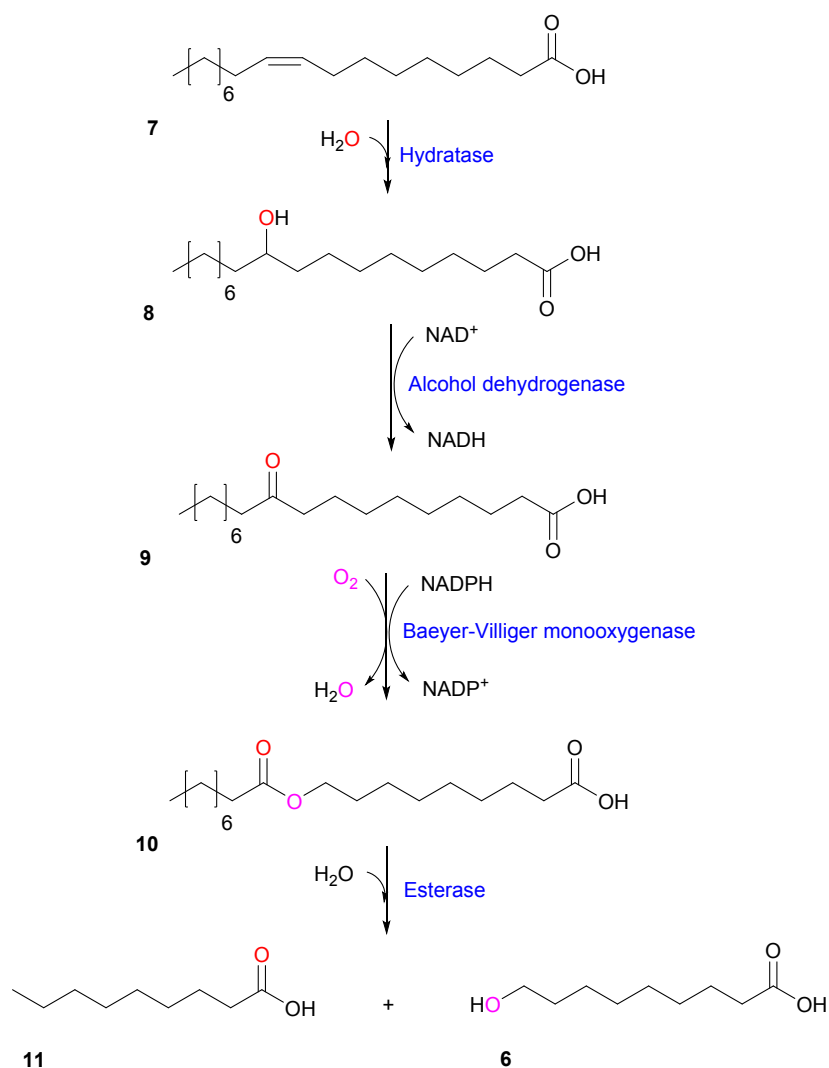
Substrate	k_{cat}/K_M ($\mu\text{M}^{-1} \text{s}^{-1}$)		
	Wild-type	Double mutant (D37S/V39S)	Quadruple mutant (D37S/A38R/V39S/T15I)
10-HOA	1.4	1.4	13
10,12-DHOA	3.5	12	2.1
12-HOA	0.61	1.5	- ^a
RA	0.13	0.21	0.02

^a not determined.

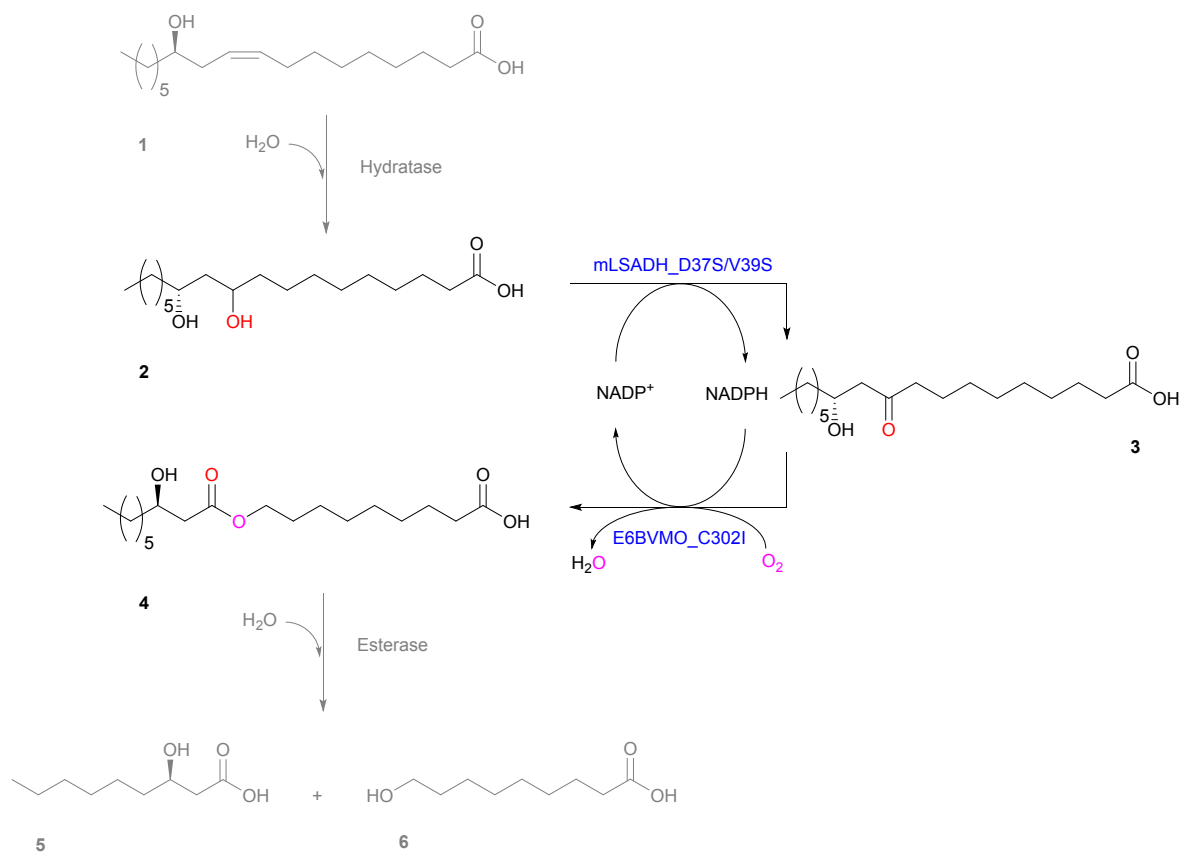
Supplementary Schemes



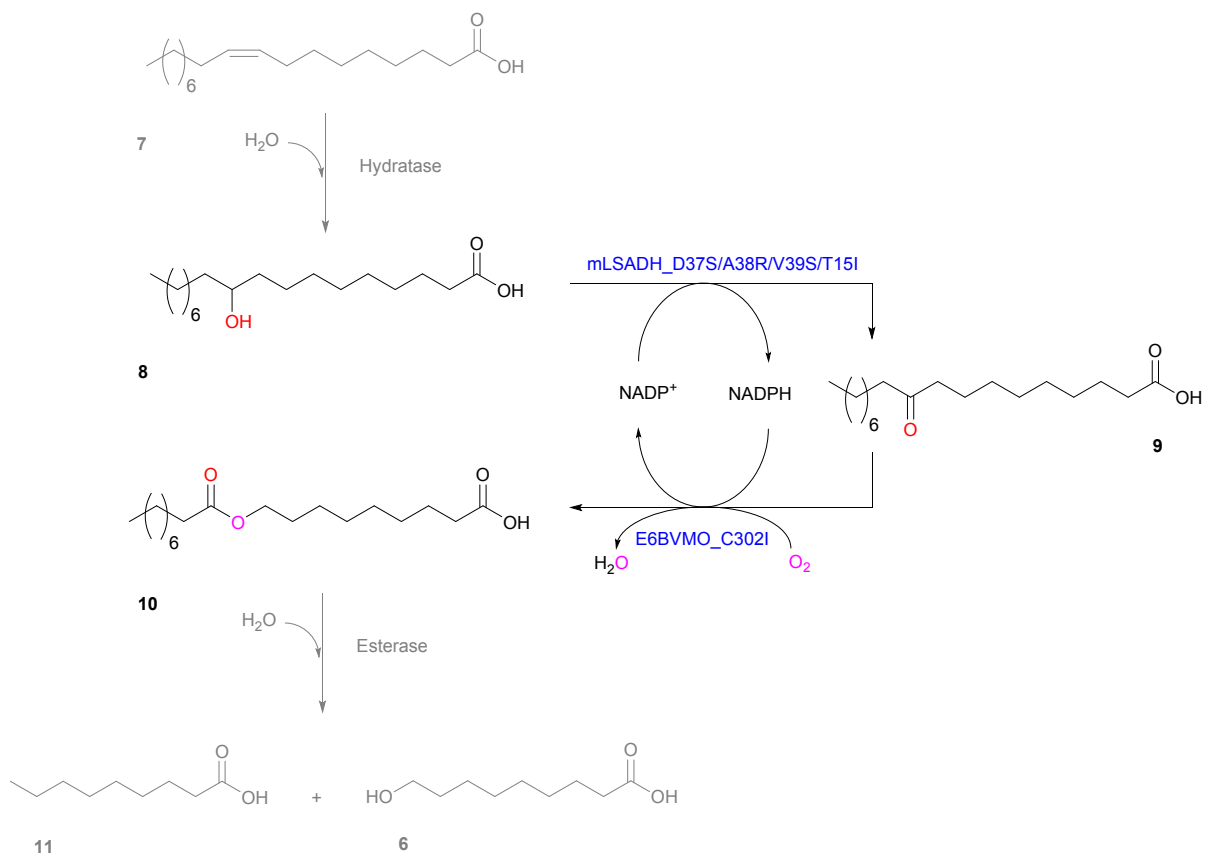
Scheme S1. Redox self-sustaining biotransformation of cyclohexanol into ϵ -caprolactone by a NADPH generating polyol dehydrogenase (PDH) and a NADPH-dependent Baeyer-Villiger cyclohexanone monooxygenase (CHMO).^{15, 16}



Scheme S2. Designed biotransformation pathway, which was constructed based on our previous study.^{5, 17} 10-Hydroxyoctadecanoic acid (**8**), which was produced from oleic acid (**7**), is enzymatically converted into 9-(nonanoyloxy)nonanoic acid (**10**) by a mLSADH and a BVMO. The resulting ester (**10**) is hydrolyzed into *n*-nonanoic acid (**11**) and 9-hydroxynonanoic acid (**6**) by an esterase.



Scheme S3. The two-step biotransformation of 10,12-dihydroxyoctadecanoic acid (**2**), which had been produced from ricinoleic acid (**1**), into 9-(12-hydroxynonanoyloxy)-nonanoic acid (**4**) by the double mutant secondary alcohol dehydrogenase (i.e., mLSADH_D37S/V39S) and a BVMO variant of *P. putida* KT2440 (E6BVMO_C302I).



Scheme S4. The two-step biotransformation of 10-hydroxyoctadecanoic acid (**8**), which had been produced from oleic acid (**7**), into 9-(nonanoyloxy)nonanoic acid (**10**) by the quadruple mutant secondary alcohol dehydrogenase (i.e., mLSADH_D37S/A38R/V39S/T15I) and a BVMO variant of *P. putida* KT2440 (E6BVMO_C302I).

Supplementary Figures

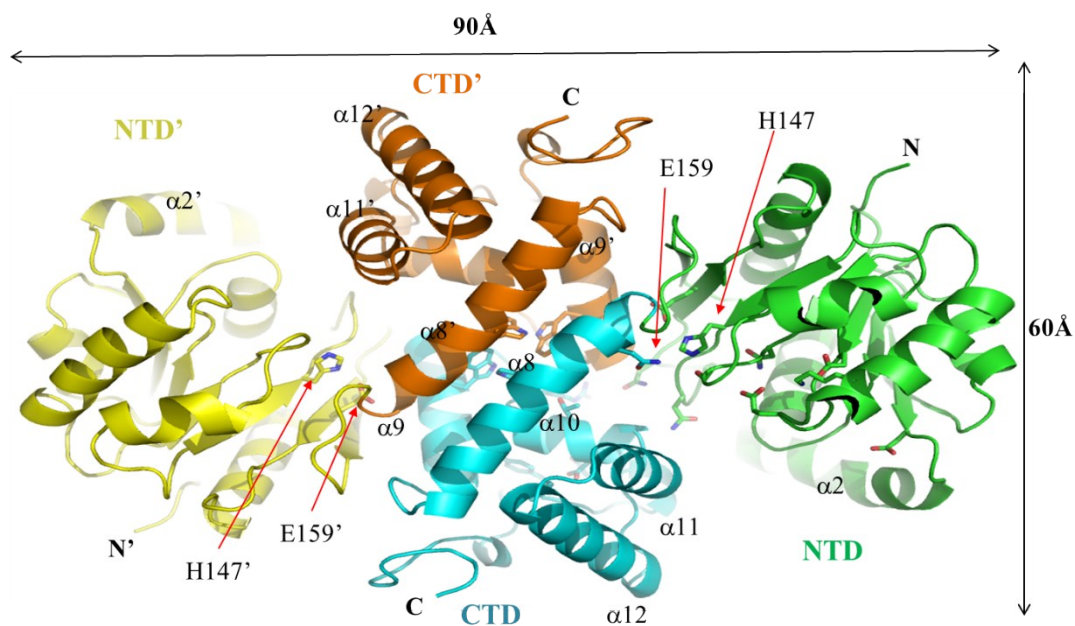


Figure S1. A cartoon representation of the mLSADH dimer in the revealed X-ray crystal structure. The N-terminal domains with the characteristic Rossmann fold are green (NTD) and yellow (NTD'), and the C-terminal helical bundle domains are cyan (CTD) and orange (CTD') in the respective monomer. The catalytic residues and some key residues at the inter-domain cleft and the dimeric interface are shown in stick models. Figure was prepared by the PyMol Molecular graphics program (Schrödinger, LLC).

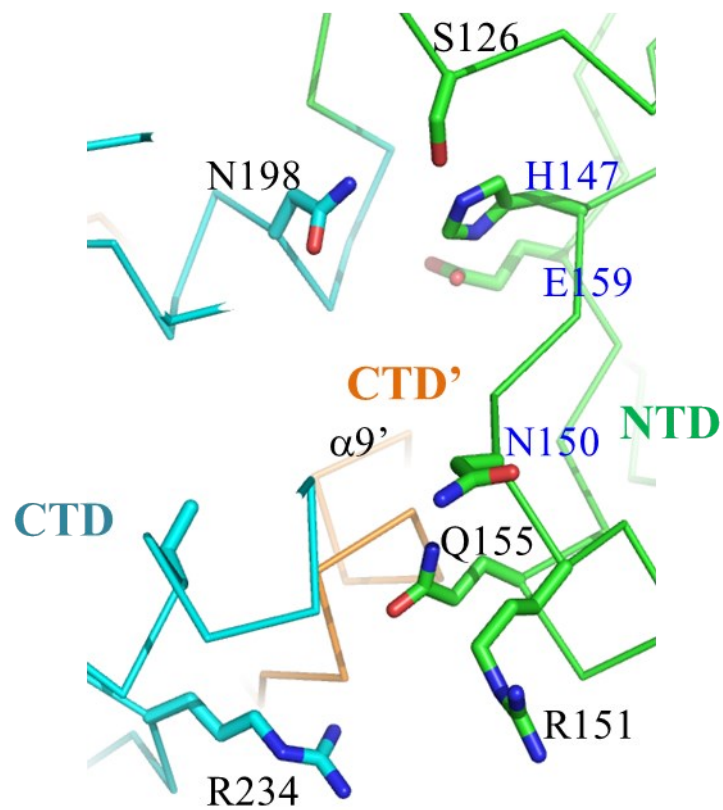


Figure S2. Active site of mLSADH. The N-terminal domain and C-terminal domain in one monomer are differentiated with green and cyan, respectively. The $\alpha 9$ -helix in the C-terminal domain of another monomer is displayed with an orange color. Some key residues at the active site and inter-domain cleft are displayed with stick models.

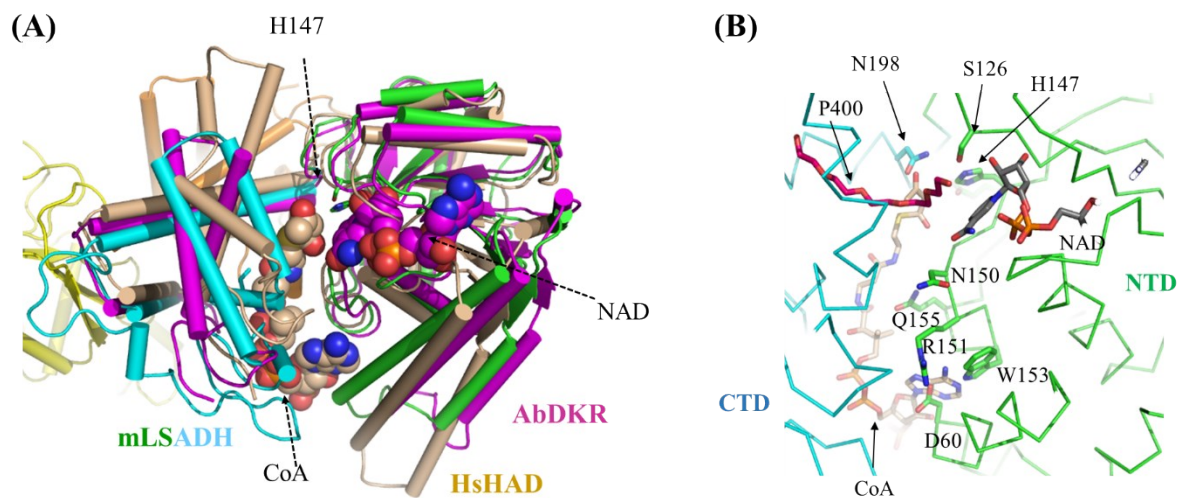


Figure S3. Active site of mLSADH with non-protein molecules found in the related proteins.

(A) Superposed structures of three related proteins. Each protein was differentiated by colors and the α -helices were drawn with cylinders. Non-protein molecules were displayed with a space-filling model and the catalytic His147 residue of mLSADH was drawn with a stick model. (B) Active site and NAD cofactor-binding site of mLSADH with non-protein molecules derived from the functionally and structurally related proteins. Some key residues at the inter-domain cleft are displayed with stick models. The non-protein molecules (CoA for acetoacetyl-CoA from HsHAD and NAD and P400 from AbDKR) were also displayed with stick models of alternating colors.

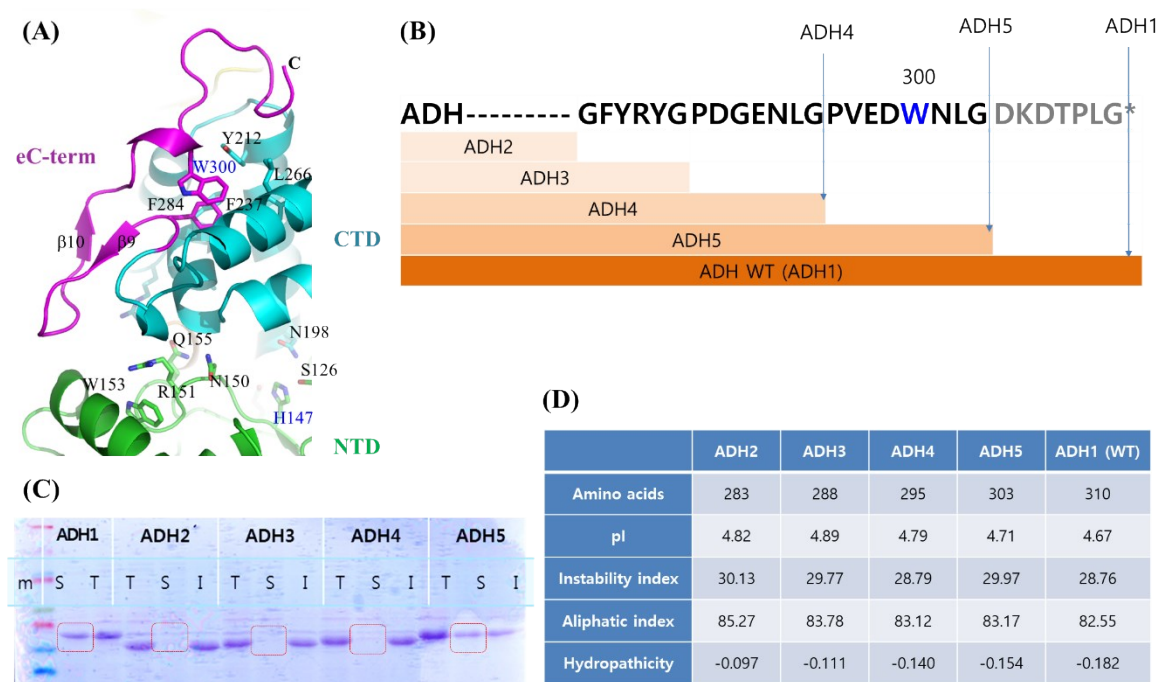


Figure S4. The extreme C-terminal region of mLSADH (Gly288-Gly310). (A) Interaction of the extreme C-terminal region (eC-term) with the remaining part of the protein. NTD, CTD and eC-term were differentiated by colors. The catalytic residues and some key residues were shown in stick models. (B) The schematic diagram for the eC-term deletion mutants. (C) The SDS-PAGE for protein stability of the eC-term deletion mutants. (D) The calculated properties of the eC-term deletion mutants. See the characterization of the eC-term (Gly288-Gly310) on page 6 for details.

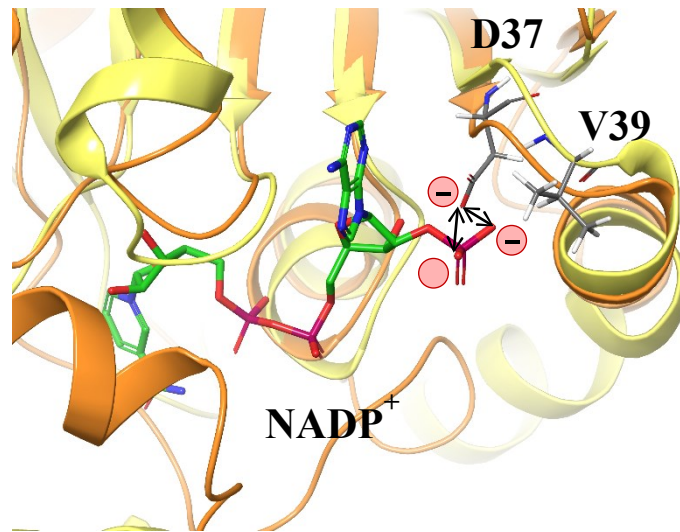
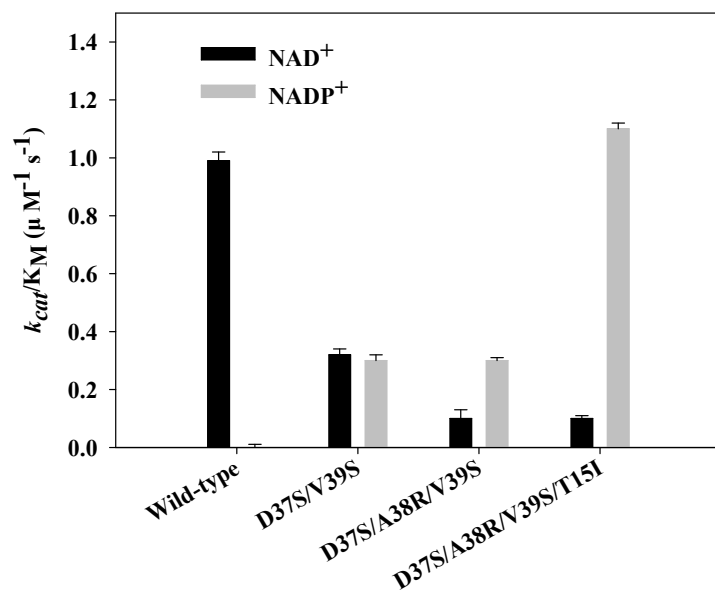


Figure S5. The superposed crystal structures of mLSADH (yellow) and cyclohexadienyl dehydrogenase (orange) from *Sinorhizobium meliloti* in complex with NADP⁺ (PDB code 4wji; rmsd 1.4 Å). NAD(P)⁺ and amino acid residues selected for mutation are shown in stick model. The possible electrostatic repulsion between the carboxylate group of mLSADH Asp37 and the phosphate moiety of the bound NADP⁺ to cyclohexadienyl dehydrogenase is shown by double-sided arrows.

(A)



(B)

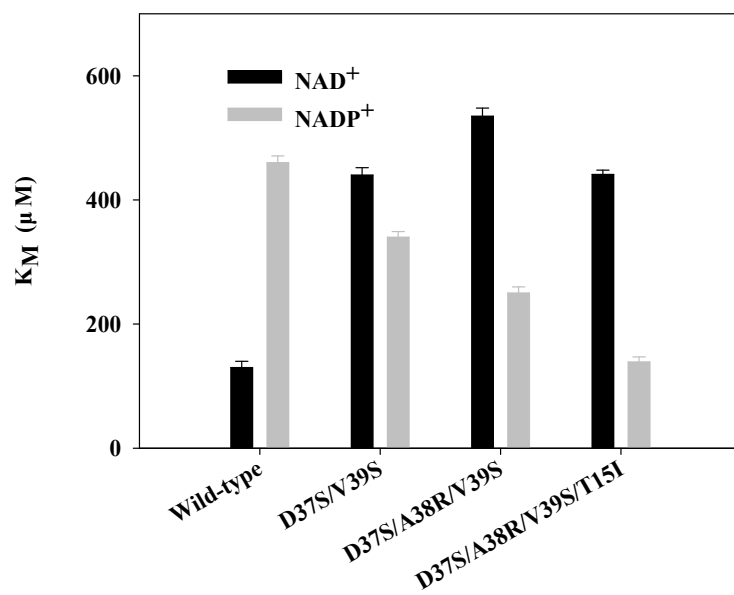


Figure S6. The k_{cat}/K_M (A) and K_M (B) values for NAD^+ (black) and NADP^+ (gray) of the purified mLSADH and its variants.

References

1. H.-J. Cha, E.-J. Seo, J.-W. Song, H.-J. Jo, A. R. Kumar and J.-B. Park, *Adv. Synth. Catal.*, 2018, **360**, 696-703.
2. E.-Y. Jeon, J.-H. Seo, W.-R. Kang, M.-J. Kim, J.-H. Lee, D.-K. Oh and J.-B. Park, *ACS Catal.*, 2016, **6**, 7547-7553.
3. E.-J. Seo, C. W. Kang, J.-M. Woo, S. Jang, Y. J. Yeon, G. Y. Jung and J.-B. Park, *Metab. Eng.*, 2019, **54**, 137-144.
4. E.-J. Seo, Y. J. Yeon, J.-H. Seo, J.-H. Lee, J. P. Boñgol, Y. Oh, J. M. Park, S.-M. Lim, C.-G. Lee and J.-B. Park, *Bioresour. Technol.*, 2018, **251**, 288-294.
5. J.-W. Song, E.-Y. Jeon, D.-H. Song, H.-Y. Jang, U. T. Bornscheuer, D.-K. Oh and J.-B. Park, *Angew. Chem., Int. Ed.*, 2013, **52**, 2534-2537.
6. Z. Otwinowski and W. Minor, in *Methods in enzymology*, Elsevier, 1997, vol. 276, pp. 307-326.
7. P. D. Adams, P. V. Afonine, G. Bunkóczi, V. B. Chen, I. W. Davis, N. Echols, J. J. Headd, L.-W. Hung, G. J. Kapral and R. W. Grosse-Kunstleve, *Acta Crystallogr. D. Biol. Crystallogr.*, 2010, **66**, 213-221.
8. P. Emsley and K. Cowtan, *Acta Crystallogr. D. Biol. Crystallogr.*, 2004, **60**, 2126-2132.
9. V. B. Chen, W. B. Arendall, J. J. Headd, D. A. Keedy, R. M. Immormino, G. J. Kapral, L. W. Murray, J. S. Richardson and D. C. Richardson, *Acta Crystallogr. D. Biol. Crystallogr.*, 2010, **66**, 12-21.
10. Schrödinger, *Schrödinger. LLC, New York, NY.*, 2017.
11. Schrödinger, *Schrödinger. LLC, New York, NY.*, 2017.

12. Schrödinger, *Schrödinger. LLC, New York, NY.*, 2017.
13. J. K. Cahn, C. A. Werlang, A. Baumschlager, S. Brinkmann-Chen, S. L. Mayo and F. H. Arnold, *ACS Synth. Biol.*, 2016, **6**, 326-333.
14. J.-M. Woo, E.-Y. Jeon, E.-J. Seo, J.-H. Seo, D.-Y. Lee, Y. J. Yeon and J.-B. Park, *Sci. Rep.*, 2018, **8**, 10280.
15. A. Kohl, V. Srinivasamurthy, D. Böttcher, J. Kabisch and U. T. Bornscheuer, *Enzyme Microb. Technol.*, 2018, **108**, 53-58.
16. F. S. Aalbers and M. W. Fraaije, *Appl. Microbiol. Biotechnol.*, 2017, **101**, 7557-7565.
17. S. Koppireddi, J.-H. Seo, E.-Y. Jeon, P. S. Chowdhury, H.-Y. Jang, J.-B. Park and Y.-U. Kwon, *Adv. Synth. Catal.*, 2016, **358**, 3084-3092.